Cell Reports Medicine, Volume *1*

Supplemental Information

Label-free, High-Resolution Optical Metabolic Imaging of Human Cervical Precancers Reveals Potential for Intraepithelial Neoplasia Diagnosis

Dimitra Pouli, Hong-Thao Thieu, Elizabeth M. Genega, Laura Baecher-Lind, Michael House, Brian Bond, Danielle M. Roncari, Megan L. Evans, Francisca Rius-Diaz, Karl Munger, and Irene Georgakoudi

SUPPLEMENTAL FIGURES AND TABLES

Supplemental Table 1. Correlation of Biological terminology to analytical process. Related to Figures 1,3-6 and STAR Methods.

Biological term	Analytical process
Epithelial thickness	Epithelial depth range between the most superficial optical section (cells clearly covering at least half of the image area below the epithelial surface or the exfoliating cell layer in healthy tissues) and the deepest optical section (cells clearly covering at least half of the image area relative to dermal components)
Differentiation gradient	Extent of epithelial morphological (cellular and nuclear) depth-dependent variability. Extracted by automated Fourier-based power spectral density (PSD) analysis, that quantifies the weighted contributions of features of different sizes. The PSD variance (square of standard deviation) for features within the 7-50μm spatial frequency range were considered. The coefficient of variation (ratio of the standard deviation to the mean) of the PSD variance over the epithelial depth was defined as the Differentiation Gradient.
Epithelial Mitochondrial Clustering Variability	Extracted by automated Fourier-based PSD analysis of processed NAD(P)H images, that reports on the spatial distribution patterns of mitochondrial formations. Variability defined by the depth-dependent variance of the mitochondrial clustering profile of each optical tissue stack within the epithelium.
Epithelial Redox Ratio average	Defined based on the NAD(P)H and FAD TPEF intensity images as the ratio FAD/ (NAD(P)H+FAD) . The average represents the epithelial RR mean value of each optical tissue stack.
Epithelial Redox Ratio Variability	Extracted by automated analysis of intensity contributions from NAD(P)H and FAD images, in a ratiometric relationship {FAD/ (NAD(P)H+FAD)}. Described by the epithelial depth-dependent variance of the RR profile of each optical tissue stack.
Epithelial Redox Ratio Heterogeneity Variability	For each optical section the pixel-based RR histogram spread (heterogeneity) was quantified by the distribution's interquartile range. The variability of the RR heterogeneity was defined by the depth-dependent variance of this parameter for each stack.

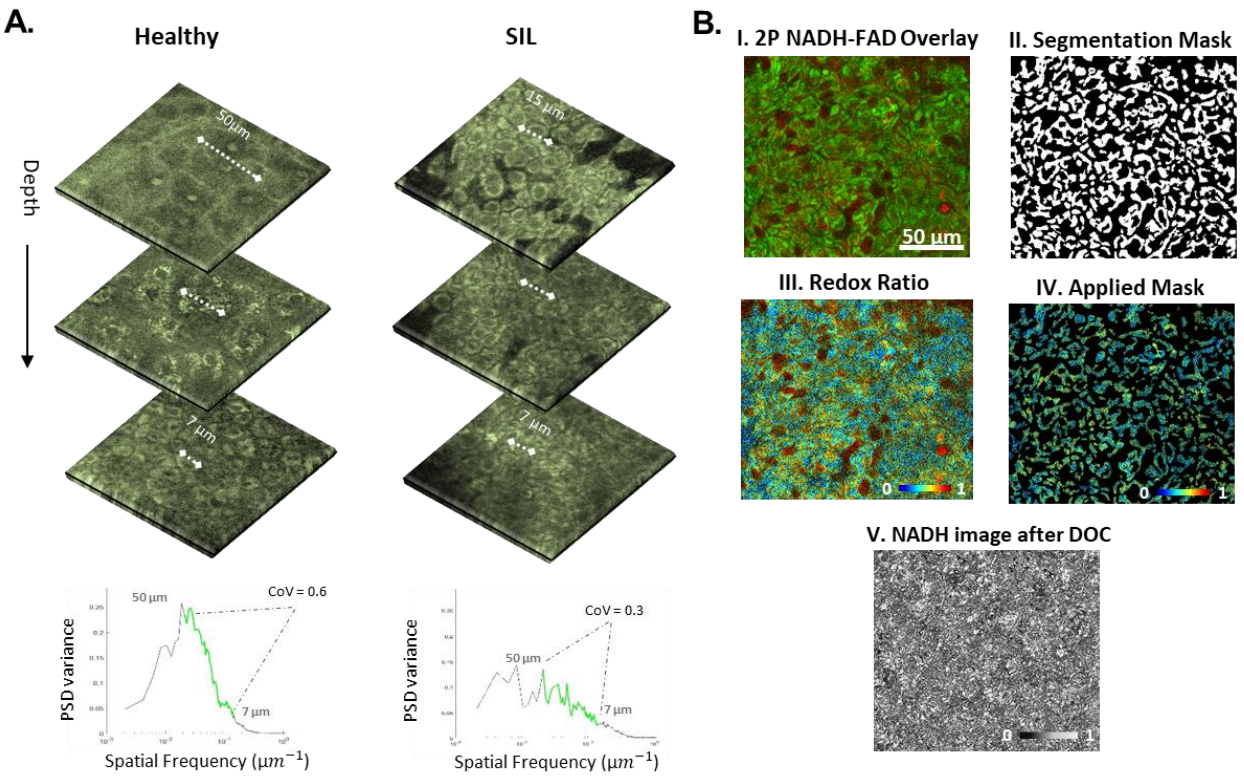

Supplemental Figure 1. Representation of analytical steps, Related to Figures 1,3,4 and STAR Methods. A. Automated image analysis for quantitative morphological depth dependent epithelial evaluation. Representative optical NAD(P)H TPEF sections acquired over depth from a Healthy and a HSIL cervical tissue, along with corresponding tissue stack PSD variance profiles. (green segments indicate spatial frequency range corresponding to image features of 7-50 microns). The coefficient of variation (CoV) extracted from each variance curve is also shown, as a quantitative metric describing herein the epithelial differentiation gradient. Cellular and nuclear sizes regress over depth in healthy tissues in a much greater extent than SIL tissues, making PSD variance metrics valuable indicators of the extent of the depth-dependent intraepithelial differentiation gradient. B. Representation of automated image analysis steps for quantitative extraction of cellular-related biomarkers. (I) Representative TPEF NAD(P)H (green) and FAD (red) overlaid fluorescence image. (II) Respective segmentation mask for isolation of cytoplasmic related-pixels and removal of saturated pixels and the nuclear and interstitial features. (III) Redox ratio map calculated as the ratio of FAD/(NAD(P)H+FAD). (IV) Example of application of segmentation mask shown in (II) to RR image map shown in (III) to report functional outcomes from cytoplasm-related pixels only. (V) Cloned NAD(P)H image after application of segmentation mask for extraction of mitochondrial organization parameter. Scale bar is same for all images of figure.

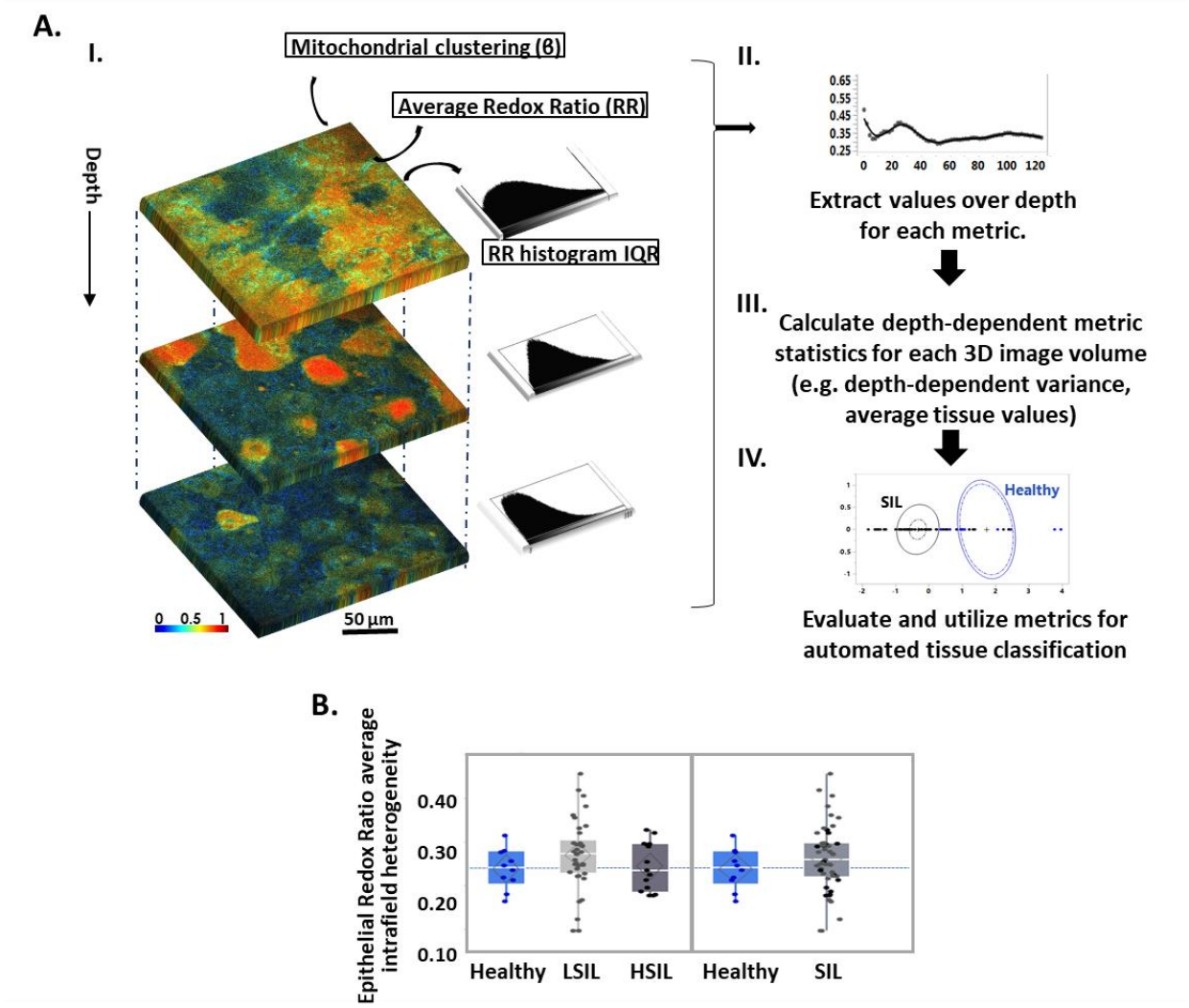

Supplemental Figure 2. Automated methodology for quantification of function, Related to Figures 1,3-6 and STAR Methods. A. (I) Extraction of relevant metrics for each optical section of the sampled epithelial volume after appropriate preprocessing steps for each marker as described in Methods. Scale bar is same for all images of panel. (II) Plotting epithelial depth-dependent profiles. (III) Calculation of epithelial depth-dependent statistical metrics. (IV) Evaluation and utilization of extracted parameters for automated classification. B. Mean overall intrafield heterogeneity redox ratio outcomes derived from the epithelial RR heterogeneity average of each optical tissue stack for the Healthy, LSIL and HSIL cervical tissues examined. Healthy versus SIL comparisons are also presented. Data are presented as quantile boxplots with median (white line) and 95% confidence diamond around the mean (gray diamond). Each point represents one optical image stack.

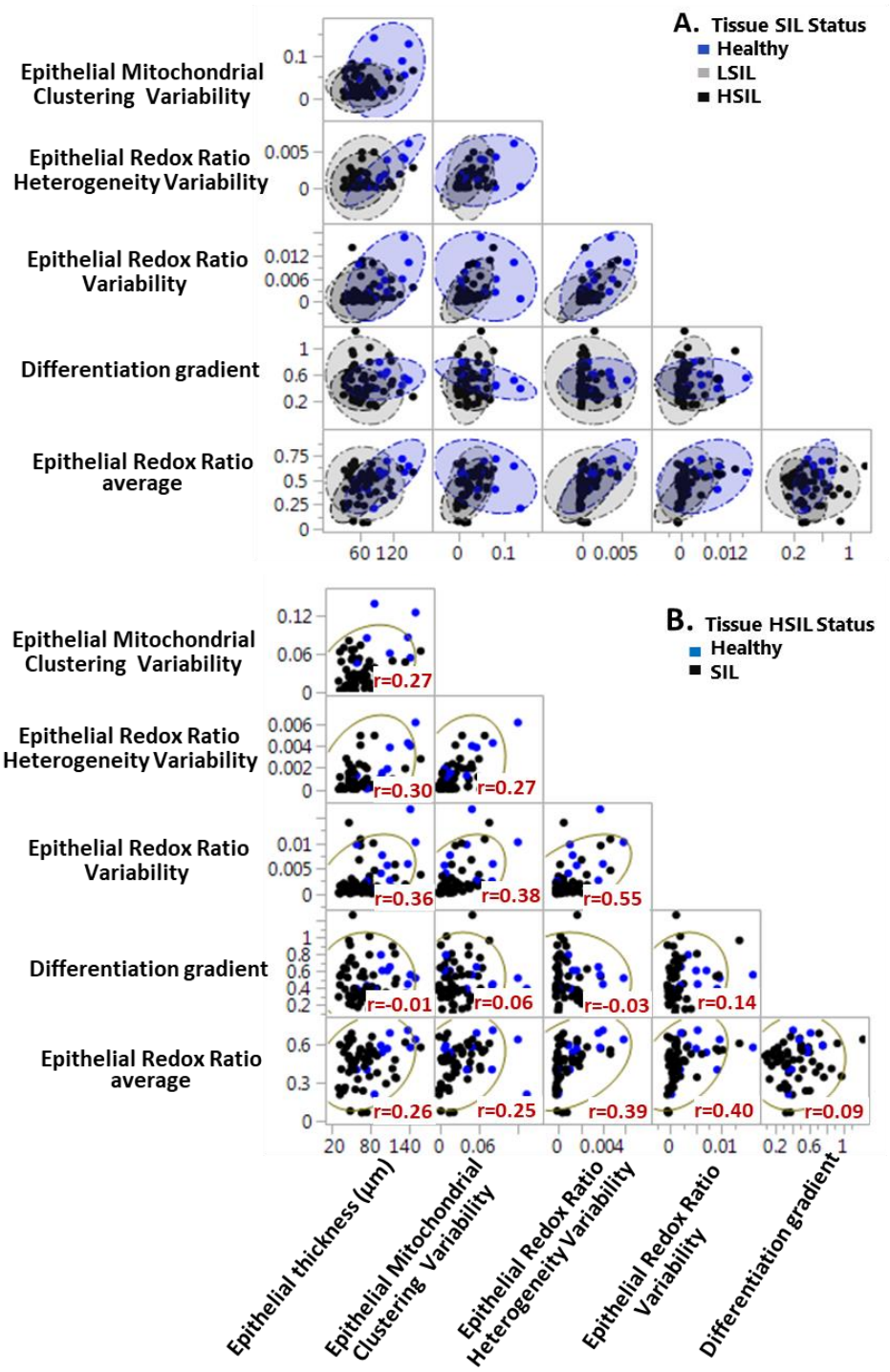

Suppl. Figure 3. Multivariate analyses, Related to Figures 5-6 and STAR Methods. A. Scatterplot Matrix reporting covariances for each classification group and each pair of covariates. Observations vary differentially across classes and covariate pairs, supporting the selection of a QDA model. B. Multicollinearity diagnostics through pairwise correlations suggest lack of multicollinearity (correlation coefficients < 0.7) indicating no offending variables. Correlations coefficients for each pair of covariates is shown within each matrix block.

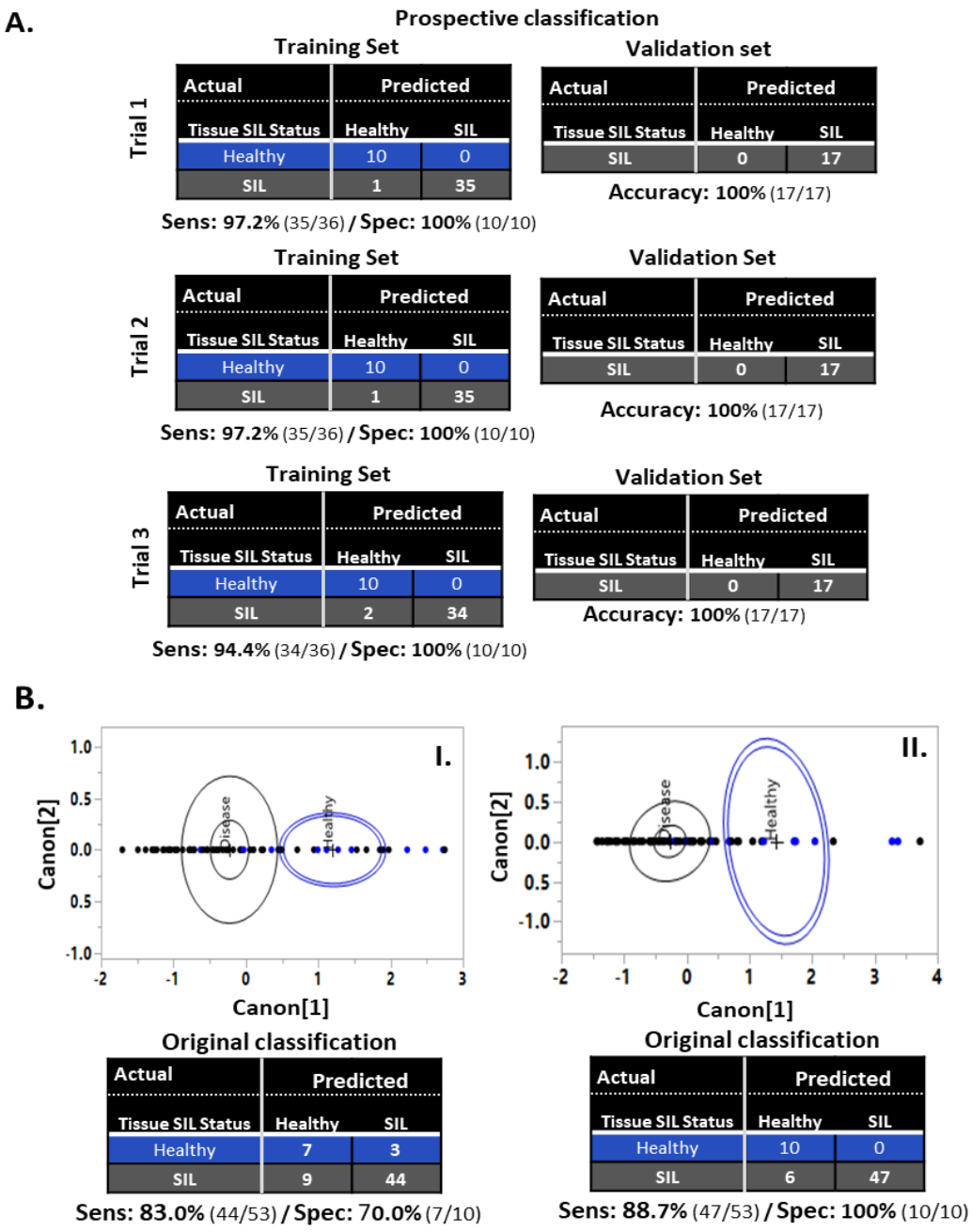

Suppl. Figure 4. QDA classidications, Related to Figures 5-6 and STAR Methods. A. Detailed outcomes for each randomized run for the predictive model as shown in summary in figure 5A for prospective classification. For each run a randomized separation 70% training SIL stacks/30% training–test SIL stacks was per performed, while the healthy stacks were always part of the training set. For each run original classification outcomes are shown for the training sets along with the prospective classification outcomes for the blinded, validating sets. B. QDA analysis at the Healthy vs. SIL levels utilizing only morphological (I) or only functional (II) markers as shown in Figures1,3-4. (top panels) Respective 2D canonical QDA scatterplots showing the tissue separation of Healthy (blue) and SIL (gray) tissue stacks. (bottom panels) Extracted sensitivity and specificity outcomes are also presented.

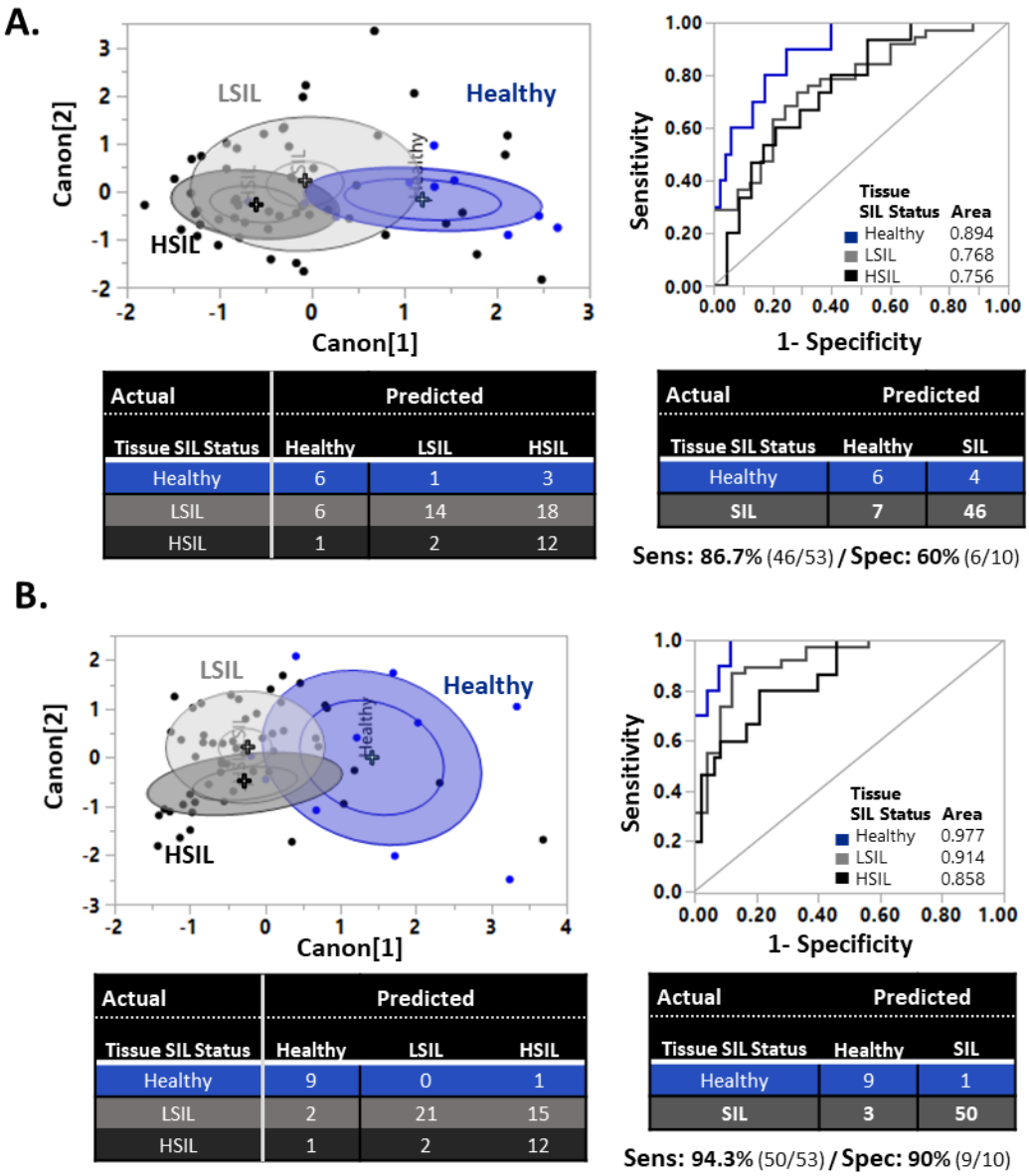

Supplemental Figure 5. QDA classidications, Related to Figures 5-6 and STAR Methods. QDA analysis at the Healthy (blue), LSIL (light gray), and HSIL (dark gray) levels utilizing only morphological (A) or only functional (B) markers as shown in Figures 1,3-4 and Suppl.Table 1. (left panel) 2D canonical QDA scatterplot showing in space the tissue separation of the Healthy (blue), LSIL (light gray), and HSIL (dark gray) tissue stacks. Colored ellipsoids represent 50% of data coverage. (right panel) ROC analysis of the QDA discrimination model at the Healthy (blue), LSIL (light gray) and HSIL (dark gray) level. Area under the ROC curve for each tissue group is also shown, indicating discrimination accuracy. (bottom panels) Original classification outcomes based on the comparison of the QDA model predictions at the Healthy (blue), LSIL (light gray) and HSIL (dark gray) level and merged classification outcomes at the Healthy (blue) and SIL (gray) level with corresponding histopathological evaluations and extracted sensitivity and specificity outcomes.

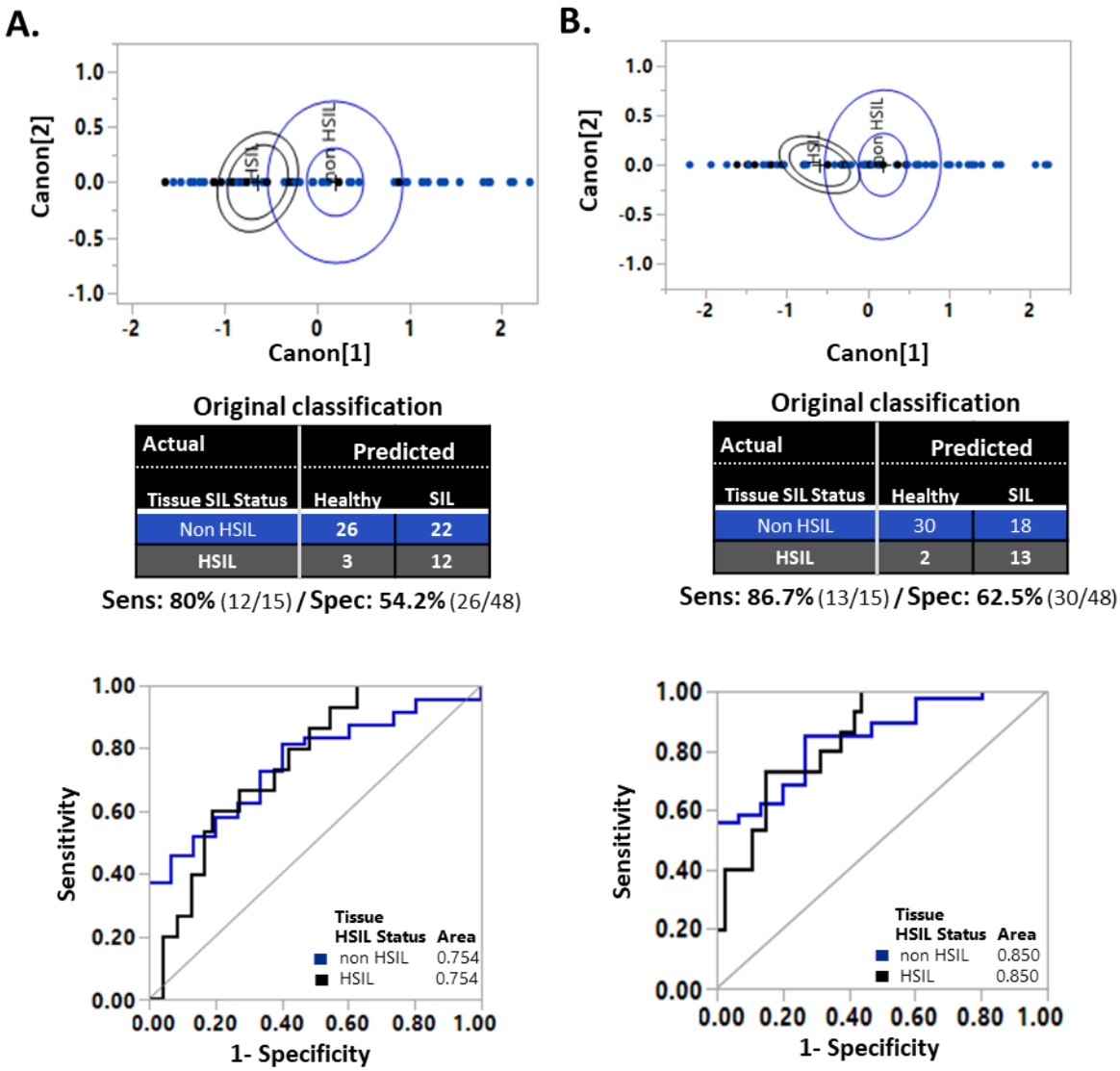

Supplemental Figure 6. QDA classidications, Related to Figures 5-6 and STAR Methods. QDA analysis at the non-HSIL vs. HSIL levels utilizing only morphological (A) or only functional (B) markers as presented in Figures 1,3-4 and Suppl.Table 1. (top panel) 2D canonical QDA scatterplot showing the tissue separation of the non-HSIL (blue) and HSIL (gray) tissue stacks. (Middle and bottom panels) Extracted sensitivity and specificity outcomes are also presented. ROC analysis of the QDA discrimination model at the non-HSIL (blue) and HSIL (gray) level. Area under the ROC curve for each tissue group is also shown, indicating discrimination accuracy.